THE ASTROPHYSICAL JOURNAL, 229:136–146, 1979 April 1

THE DEPLETION OF INTERSTELLAR GASEOUS IRON

BLAIR D. SAVAGE*
Washburn Observatory, University of Wisconsin–Madison
AND
RALPH C. BOHLIN*
Goddard Space Flight Center, Greenbelt, Maryland
Received 1978 April 21; accepted 1978 September 21

ABSTRACT

The *Copernicus* ultraviolet telescope was used to measure equivalent widths of interstellar Fe II resonance lines toward 55 early-type stars. The measurements permit the determination of Fe II column densities. The depletion of interstellar gaseous iron was obtained by combining these measurements with the results from a previous atomic and molecular hydrogen survey program. The derived depletions mostly refer to matter in H I regions. The average gaseous iron abundance ratio for all the objects is $\langle \mathrm{Fe/H} \rangle = \sum N(\mathrm{Fe\ II}) / \sum N(\mathrm{H\ I} + \mathrm{H_2}) = 4.5 \times 10^{-7}$, which implies an average depletion of $\delta = 0.018$. However, the variations about this average are large, with the extreme cases being $\delta = 0.78$ for the intermediate-velocity cloud toward HD 93521 and $\delta = 0.0032$ for the dark cloud star ρ Oph. Regional differences in iron depletion are observed; two Cygnus stars have $\langle \delta \rangle = 0.039$, while 10 Scorpius-Ophiuchus stars have $\langle \delta \rangle = 0.0091$. The amount of iron depletion correlates roughly with variations in the ultraviolet extinction properties of grains but does not correlate with various other parameters characterizing interstellar grains. The iron depletion correlates with several indicators of cloud density in the sense that depletion is greatest (smallest δ) in the densest interstellar regions. The interrelationships between N(Fe II) and other heavy-element column densities suggest that Fe, Ca, Mn, and Ti probably exist in grains with similar formation and/or destruction properties. Iron depletion is found to be less in the clouds toward distant high-latitude stars. The nearly normal gaseous iron abundance in the distant high-latitude intermediate-velocity cloud toward HD 93521 is consistent with the idea that these clouds are produced by galactic supernova explosions.

Subject headings: interstellar: abundances — interstellar: matter

I. INTRODUCTION

Studies of the depletion of interstellar elements from the gas phase have provided an indirect but powerful method for studying the interstellar dust. The term depletion, δ, refers to the factor by which the gas phase column density of an element is below that expected on the basis of a measured total hydrogen column density and the asumption of cosmic abundances. The missing gas is assumed to be in the solid phase, since observed molecular column densities can explain only a very small part of the depletion. The study of depletion has been greatly expanded by the unique observing capabilities of the *Copernicus* ultraviolet telescope (see Spitzer and Jenkins 1975). For more recent ultraviolet and visual results see Shull, York, and Hobbs (1977), Snow (1975), and Stokes and Hobbs (1976). From these and other studies the following results have emerged.

1. The amount of elemental depletion varies from essentially no depletion ($\delta \approx 1$) for elements such as S and Zn, to depletions of 10^{-2} to 10^{-3} for Al, Ti, and Ca. For the very important C, N, and O group, depletions in the range 1 to 0.1 are indicated, although the results are very uncertain for C and N due to large curve of growth uncertainties. In the case of O, the recent detection of the weak 1355.6 Å intersystem transition in the spectrum of ζ Oph by Zeippen, Seaton, and Morton (1977) implies δ lies between 0.56 and 0.31. However, de Boer (1979) reanalyzed these data and concluded, on the basis of detailed curve-of-growth considerations, that the oxygen toward ζ Oph is depleted by only 25%.

2. The amount of depletion correlates roughly with T_c, an element's condensation temperature (Field 1974). T_c is defined as the temperature at which half of a particular atom has condensed out of a gas of solar composition as it is slowly cooled but maintained in thermal and chemical equilibrium. However, an alternate view by Snow (1975) is that the correlation is really with the first ionization potential, which is a measure of an element's chemical and physical activity.

3. The amount of depletion varies from cloud to cloud; smaller depletions (larger δ's) are recorded in the low-density intercloud regions (York 1975), in the intermediate- and high-velocity clouds (Shull, York, and Hobbs 1977), and in high-latitude clouds (Cohen

* Guest Investigator with the Princeton University telescope on the *Copernicus* satellite, which is sponsored and operated by the National Aeronautics and Space Administration.

1974; Stokes and Hobbs 1976). Larger depletions (smaller δ's) appear to be recorded in the denser interstellar clouds (Snow 1975).

4. While both Ti and Ca exhibit large and variable depletions from object to object, the column densities of Ti II and Ca II are well correlated (Stokes 1978). In contrast, N(Ti II) and N(Ca II) correlate poorly with N(Na I) and N(K I).

The systematics of depletion from element to element or object to object can provide important clues about the composition of interstellar dust and the formation and/or destruction of the grains. The purpose of the present paper is to examine the depletion of one important element in a large sample of stars in order to search for new systematic effects in the behavior of depletion. In this paper, the gas phase column density of Fe II has been determined toward 55 of the H I/H_2 survey stars of Savage *et al.* (1977, hereafter Paper I) and Bohlin, Savage, and Drake (1978, hereafter Paper II). Forty-three of these column densities are new, while the remaining 12 have been taken from previous papers based on *Copernicus* observations. In § II the observations and reduction techniques are discussed, and in § III the derived depletions are compared with a variety of cloud and dust parameters.

II. OBSERVATIONS AND DERIVATION OF N(Fe II)

The Fe II measurements were obtained as part of the H I/H_2 survey program of Papers I and II. In this program the *Copernicus* U2 phototube was used to scan the Lα line at 1216 Å, while the U1 phototube simultaneously scanned the H_2 (1, 0) band near 1093 Å. Since the Lα scanning required approximately twice as much time as the H_2 scanning, it was decided to use the available U1 scanning time to observe with a resolution of 0.05 Å the Fe II resonance lines at 1121.987, 1133.678, and 1144.946 Å. Oscillator strengths for the three lines are estimated to be: $f_{1122} = 0.020$, $f_{1134} = 0.0063$, and $f_{1145} = 0.15$ (de Boer *et al.* 1974). All observations were made with double-standard routines which produced scans approximately 0.6 Å long, centered on the line of interest. Step sizes and integration times were 0.025 Å and 14 s, respectively (Rogerson *et al.* 1973). For 19 stars all three lines were scanned: λ1122 twice, λ1134 four times, and λ1145 twice. For 24 stars only the two weaker lines were scanned, λ1122 three times and λ1134 six times. Stray light entering through the spectrograph venting hole was blocked with the U2 dipping mirror. The multiple scans were stacked and plotted with a scale suitable for direct planimeter measurements of the equivalent width, W_λ. Radiation belt particle counts were estimated with the Princeton data reduction programs. The scattered light correction was assumed to be 5% of the continuum.

Table 1 gives the measured equivalent widths along with an estimate of the 1 σ uncertainty due only to photon statistics. These errors were estimated with the expression derived by Jenkins *et al.* (1973). Uncertainties in the continuum placement will increase the actual errors, particularly for stars with relatively low $v \sin i$. In a number of cases, the profiles are complex due to multiple interstellar cloud components (see comments to Table 1). However, unless otherwise noted, the measurements refer to the entire equivalent width. At a resolution of 0.05 Å or 13 km s^{-1}, component separation is difficult except in cases where the structure is simple with a large velocity separation between components.

Column densities for all the objects listed in Table 1 were derived by fitting the measured equivalent widths to one-component Doppler-broadened curves of growth characterized by the Doppler parameter b (km s^{-1}). When only two equivalent widths are available this method is equivalent to the doublet ratio method often used to derive column densities for interstellar Na I and Ca II. The adopted method allows for the effects of saturation but is not exact, since most lines of sight to O and B stars pass through more than one cloud. As the degree of line saturation increases the errors associated with the method increase (Nachman and Hobbs 1973). To provide a guide to the amount of line saturation, we have listed in Table 1 the central depth in percent of the weakest Fe II line at 1134 Å. Eighty percent of the objects have A_c less than 50%. However, the *Copernicus* resolution of 13 km s^{-1} is about 3 or 4 times larger than the full width at half-intensity of typical cloud line profiles, and the true central depths will be larger than those listed. Some information on curve-of-growth uncertainties for individual stars in this program can be obtained by referring to the higher-resolution optical data for Ti II (Stokes 1978) and Ca II (Marschall and Hobbs 1972). These data are particularly useful for identifying the multicomponent nature of most lines of sight. By allowing for instrumental smearing effects, it appears that the Fe II 1134 Å line exhibits roughly the same degree of saturation as the Ca II K line observed in high resolution. This is important, since the doublet ratio method applied to the moderately saturated Ca II doublet has generally yielded results consistent with more precise integrations over optical depth of the high-resolution observations (e.g., compare the Ca II column densities listed in Savage and Jenkins 1972 with those listed in Hobbs 1974). For particular objects it would be possible to use the optical data as a guide in producing detailed fits to the *Copernicus* Fe II line profiles. But such a procedure is well beyond the scope of this survey program. It is difficult to estimate errors when dealing with complex curve-of-growth uncertainties. Therefore the reader should carefully consider the implications of the central depths listed in Table 1. For A_c (1134) $\lesssim$ 30% the results should be reliable (logarithmic errors $\lesssim$0.2). As A_c (1134) becomes larger the errors will increase, particularly in those cases where the optical data on Ti II and Ca II imply numerous cloud components.

The results are given in Table 2 along with Fe II measurements collected from several previous publications. The various columns contain the following information: (1) HD number, (2) name, (3) galactic

TABLE 1

Fe II EQUIVALENT WIDTHS

HD	W_λ (1133.678) (mÅ)	W_λ (1121.987) (mÅ)	W_λ (1144.946) (mÅ)	A_c (1133.678) (%)	REMARKS
2905	57.9 ± 3.7	106.0 ± 9.0	-	50	
21856	31.6 ± 2.2	73.4 ± 6.3	-	41	
22951	30.2 ± 1.8	40.7 ± 3.3	-	41	
34989	31.4 ± 1.8	58.4 ± 3.2	-	38	
35149	15.1 ± 1.8	30.9 ± 3.1	68.5 ± 2.8	18	
36822	22.8 ± 1.3	42.0 ± 1.8	80.1 ± 1.9	29	Uncertain continuum for λ 1145
48099	77.7 ± 6.5	123.0 ±12.0	-	71	
53975	63.8 ± 3.8	136.0 ± 7.0	-	46	
54662	35.5 ± 6.0	98.5 ±13.0	-	40	
55879	18.9 ± 2.6	64.7 ± 3.5	-	26	
57682	46.0 ± 2.6	102.0 ± 4.0	-	31	Uncertain continuum for λ 1122 and λ 1134
74375	22.9 ± 1.2	45.6 ± 2.3	-	33	
93521b	26.4 ± 2.6	75.1 ± 5.3	-	19	Two resolved components, $\lambda_a - \lambda_b \approx 0.16$Å
a	18.5 ± 2.4	48.9 ± 5.3	-	27	
99171	23.6 ± 2.3	43.7 ± 4.2	-	24	
112244	46.3 ± 4.8	113.0 ± 7.0	168.0 ± 6.0	45	Two components, $\Delta\lambda \approx 0.065$Å
113904B	73.8 ± 5.9	181.0 ± 9.0	286.0 ± 7.0	45	Wide and complex profile
135591	38.6 ± 1.9	88.1 ± 4.1	129.0 ± 3.0	45	
141637	28.8 ± 2.3	61.5 ± 3.6	104.0 ± 3.0	36	
144217	29.1 ± 0.9	52.3 ± 1.2	99.0 ± 1.0	34	
144470	26.6 ± 1.2	58.4 ± 2.1	104.0 ± 2.0	34	Two components, $\Delta\lambda \approx 0.06$Å
145502	27.0 ± 2.5	48.2 ± 3.3	95.6 ± 4.1	36	Two components, $\Delta\lambda \approx 0.05$Å
147165	37.9 ± 0.7	59.0 ± 1.3	-	54	
147933A	-	66.6 ± 7.2	100.0 ± 9.0	-	W_λ (1142.33) = 33mÅ (Snow private communication) N(Fe II) based on all lines, $f_{1142} = 0.0069$
148184	32.9 ± 4.1	70.9 ± 7.0	121.0 ± 6.0	38	
148605	17.3 ± 1.3	43.5 ± 2.6	84.8 ± 2.9	25	
149881	61.0 ± 5.4	154.0 ±12.0	-	57	
150898	46.7 ± 2.7	81.9 ± 7.8	135.0 ± 6.0	52	
155806	39.1 ± 2.3	85.7 ± 4.3	-	48	
164402	45.0 ± 3.1	100.0 ± 7.0	155.0 ± 7.0	58	Uncertain continuum for λ 1145
165024	26.7 ± 1.2	47.6 ± 2.1	99.6 ± 3.1	36	
167263	43.2 ± 3.3	72.9 ± 6.1	-	50	
167264	32.0 ± 2.5	77.4 ± 7.2	-	46	Uncertain continuum for λ 1122
184915	28.1 ± 2.7	-	161.0 ± 6.0	29	λ1122 contaminated
188209	50.1 ± 3.5	126.0 ± 7.0	198.0 ± 7.0	46	
188439	36.0 ± 4.3	106.0 ±11.0	-	38	
193322	69.2 ±12.0	-	174.0 ±18.0	67	
203064	48.4 ± 2.8	77.6 ± 4.3	109.0 ± 4.0	49	
204172	72.9 ± 1.1	157.0 ± 3.0	-	64	Uncertain continuum for λ1122
209975	48.5 ± 3.4	93.6 ± 7.7	-	63	
214080	41.1 ± 6.1	90.5 ±13.0	-	38	Complex profile
218376	33.9 ± 2.7	60.3 ± 3.9	-	44	
219188	43.1 ± 4.7	117.0 ±11.0	-	43	
224572	22.9 ± 2.2	62.0 ± 4.0	-	29	

TABLE 2

Fe II COLUMN DENSITIES

HD	NAME	ℓ	b	S. T.	E(B-V) (mag.)	r (pc)	log N(Fe II) (cm^{-2})	b ($km\ s^{-1}$)	log N(HI + H_2) (cm^{-2})	- log δ	- log f	n(HI + H_2) (cm^{-3})	E(1330-V)/E(B-V)	log N(Ti II) (cm^{-2})
(1)	(2)	(3)	(4)	(5)	(6)	(7)	(8)	(9)	(10)	(11)	(12)	(13)	(14)	(15)
2905	κ Cas	121	0	B1 Ia	.35	1009	15.05	12.0	21.30	1.65	.72	.64	6.30	12.14 M
21856	-	156	-17	B1 V	.19	581	14.71	12.0	21.12	1.73	.77	.74	-	-
22951	40 Per	159	-17	B1 IV	.24	406	14.97	3.5	21.23	1.66	.46	1.3	-	11.82 M
23180	o Per	160	-18	B1 III	.30	239	14.34 H	-	21.21	2.27	.30	2.2	-	11.48 M
24398	ζ Per	162	-17	B1 Ib	.33	394	14.25 I	-	21.20	2.35	.23	1.3	4.97	11.29 M
28497	-	209	-37	B1.5 Ve	.02	466	14.25 G	-	20.20	1.35	5.08	.11	-	-
34989	-	195	-16	B1 V	.13	603	14.79	6.5	21.11	1.72	>2.36	.69	3.54	-
35149	23 Ori	199	-18	B1 Vn	.11	429	14.42	4.5	20.74	1.72	>1.91	.42	6.18	-
36822	ϕ^1 Ori	195	-13	B0.5 IV-V	.11	413	14.62	5.0	20.84	1.62	1.21	.54	4.77	-
38666	μ Col	237	-27	09.5 V	.01	701	14.04 G	-	19.85	1.21	4.04	.032	-	-
37742	ζ Ori	206	-17	09.7 Ib	.08	352	13.90 C	-	20.41	1.91	4.38	.24	-	11.23 M
48099	-	206	1	07 V	.27	1169	15.25	12.0	21.25	1.40	.66	.50	7.33	-
50896	-	235	-10	WN5 + B	.14	1393	14.63 F	-	20.59	1.36	1.00	.091	-	-
53975	-	226	-2	07.5 V	.22	1334	15.05	18.0	21.16	1.51	1.62	.35	5.19	-
54662	-	224	-1	06.5 V	.35	1236	14.73	25.0	21.41	2.08	1.11	.68	5.83	12.02 K
55879	-	225	0	B0 III	.10	1462	14.42	>30.0	20.90	1.88	>1.70	.18	-	-
57682	-	224	3	09 IV	.12	1614	14.89	16.0	20.87	1.38	>1.62	.15	-	-
74375	-	276	-11	B1.5 III	.10	348	14.61	6.0	20.82	1.61	>2.18	.62	-	-
93521	-	183	62	09 Vp	.03	1778	14.44(a)	14.0	20.11	0.69(a+b)	>1.27	.023	-	-
							14.59(b)	22.0						
99171	-	286	17	B2 IV-V	.05	470	14.66	4.8	20.65	1.39	5.10	.31	-	-
112244	-	304	6	08.5 Iaf	.34	1854	14.89	14.0	21.17	1.68	.73	.26	-	-
113904B	θ Mus	305	-2	09 II	.29	1276	15.10	23.0	21.13	1.43	1.00	.34	-	-
116658	α Vir	316	51	B1 IV	.03	86	13.4 A	-	<19.0	<1.00	-	<.038	-	10.69 M
122451	β Cen	312	1	B1 III	.00	84	13.97 A	-	19.52	.95	5.42	.13	-	-
135591	-	320	-3	07.5 IIIf	.22	1178	14.85	10.0	21.12	1.67	1.05	.36	-	-
141637	1 Sco	346	22	B1.5 Vn	.20	232	14.70	8.0	21.20	1.90	1.67	2.2	5.05	-
143018	π Sco	347	20	B1 V + B2	.08	171	14.04 A	-	20.75	2.11	1.13	1.1	-	10.90 M
144217A	β^1 Sco	353	24	B0.5 V	.20	161	14.72	6.5	21.14	1.82	1.01	2.8	4.40	11.23 M
144470	ω^1 Sco	353	23	B1 V	.22	227	14.65	8.0	21.24	1.99	.89	2.5	4.10	11.44 M
145502	ν Sco	355	23	B2 IVp	.27	174	14.68	6.5	21.19	1.91	1.00	2.9	3.33	11.46 M
147165	σ Sco	351	17	B1 III	.38	142	14.93	5.5	21.37	1.84	1.28	5.3	2.40 D	11.52 M
147933A	ρ Oph	354	18	B2 IV	.47	174	14.71	9.0	21.86	2.50	1.00	13.0	3.26	-
148184	χ Oph	358	21	B1.5 Ve	.53	134	14.76	9.0	21.35	1.99	.42	5.5	3.79	11.80 L
148605	22 Sco	353	16	B2 V	.10	217	14.45	7.0	20.96	1.91	1.92	1.4	3.00	-
149757	ζ Oph	6	24	09.5 Vnn	.32	138	14.56 B	-	21.15	1.99	.20	3.3	6.50	11.48 M
149881	-	31	36	B0.5 III	(.12)	1614	14.96	30.0	20.65	1.09	>1.35	.090	-	-
150898	-	330	-8	B0.5 Ia	.18	2323	14.96	9.0	21.01	1.45	.90	.14	5.71	-
155806	-	353	3	07.5 Vne	.33	735	14.83	12.0	21.14	1.71	.91	.60	-	-
157246	γ Ara	353	-11	B1 Ib	.08	689	14.43 E	-	20.71	1.48	1.18	.24	-	-
158926	λ Sco	352	-2	B1.5 IV	.03	102	13.5 J	-	19.38	1.28	6.38	.076	-	<10.79 M
164402	-	7	0	B0 Ib	.28	1738	14.88	14.0	21.13	1.65	1.34	.25	-	-
165024	θ Ara	343	-14	B2 Ib	.10	745	14.66	6.5	20.85	1.59	>1.60	.31	-	-
167263	16 Sgr	11	-2	09.5 II-IIIn	.31	1349	14.95	7.5	21.18	1.63	.69	.36	-	-
167264	15 Sgr	10	-2	B0 Ia	.34	1556	14.70	14.0	21.25	1.95	.67	.37	3.97	-
184915	κ Aq1	32	-13	B0.5 IIIn	.26	630	14.63	14.0	21.08	1.85	.47	.62	5.57	-
188209	-	81	10	09.5 Iab	.21	2014	14.99	14.0	21.00	1.41	.70	.16	8.00	12.28 K
188439	-	82	10	B0.5 IIIn	.14	1358	14.72	>30.0	20.89	1.57	.64	.19	-	-
193322AB	-	78	3	09V:n	.40	608	15.16	12.0	21.16	1.40	.77	.77	6.73	-
203064	68 Cyg	88	-4	07.5 III:nf	.28	893	15.05	7.0	21.14	1.49	.55	.50	6.24	-
204172	69 Cyg	83	-10	B0 Ib	.17	2118	15.11	18.0	21.03	1.32	1.13	.17	7.61	-
209975	19 Cep	105	5	09.5 Ib	.38	1086	14.95	11.0	21.19	1.64	.80	.46	-	-
214080	-	45	-57	B1 Ib	.08	3404	14.85	13.0	20.64	1.19	>1.34	.042	-	-
218376	1 Cas	110	-1	B0.5 III	.22	621	14.84	6.5	21.07	1.63	.62	.62	6.04	11.88 M
219188	-	83	-50	B0.5 II-IIIn	(.09)	2355	14.82	30.0	20.87	1.45	1.23	.10	-	-
224572	σ Cas	116	-6	B1 V	.17	377	14.53	14.0	21.04	1.91	.51	.94	-	-

REFERENCE CODE

A - de Boer et al. (1974)
B - Morton (1975)
C - Olthof and Pottasch (1975)
D - Bless and Savage (1972)
E - Morton and Hu (1975)
F - Shull (1977)
G - Shull and York (1977)
H - Snow (1976)
I - Snow (1977)
J - York (1975)
K - Wallerstein and Goldsmith (1974)
L - de Boer and Pottasch (1974)
M - Stokes (1978)

longitude and (4) latitude, (5) spectral type, (6) $E(B-V)$, (7) r, the distance in pc, (8) log N(Fe II), where N(Fe II) is the Fe II column density in atoms cm^{-2}, (9) b, the curve-of-growth Doppler parameter in km s^{-1}, (10) log N(H I + H_2), where N(H I + H_2) = N(H I) + $2N(H_2)$ is the total hydrogen density, (11) $-\log\delta = \log N(\text{H I} + H_2) - \log N(\text{Fe II}) - 4.6$, where δ is the depletion factor, (12) $-\log f$, where $f = 2N(H_2)/N(\text{H I} + H_2)$, (13) $n(\text{H I} + H_2) = N(\text{H I} + H_2)/r$, the *average* line-of-sight total hydrogen space density in atoms cm^{-3}, (14) $E(1330-V)/E(B-V)$ where $E(1330-V)$ is the color excess between 1330 Å and the photoelectric V band, and (15) log N(Ti II), where N(Ti II) is the interstellar Ti II column density. The entries for columns (5), (6), (7), (10), (12), and (13) are from Paper I. Except where noted, the color excess ratio $E(1330-V)/E(B-V)$ was obtained from *OAO 2* broad-band photometry (Code, private communication). The reference code at the bottom of the table provides the sources for the various entries in columns (8), (14), and (15). In deriving the depletion factor, δ, given in column (11), we used the solar abundance of iron from Withbroe (1971). Pagel (1974) has indicated that, with only a few exceptions, the solar abundance scale is nearly indistinguishable from the "cosmic abundances" found in the O and B stars. The distances to the stars were listed with an unreasonable precision to allow the reader to easily check those derived quantities that depend on distance.

Observations of interstellar Fe II lines for 10 other stars were obtained as part of this survey program. However, for a variety of reasons these data were rejected from consideration. In some situations stellar blending seriously compromised the interstellar measurements, while in other cases the object faintness resulted in spectra with very low signal-to-noise ratio.

After reading a preliminary draft of this paper K. S. de Boer brought to our attention the possibility of blending between interstellar C I lines and the Fe II line at 1121.987 Å. The troublesome C I lines are: $(2p^2)^3P_1$–$(9s)^1P_1$, 1121.920 Å; $(2p^2)^3P_2$–$(8d)^3P_1$, 1121.998 Å; and $(2p^2)^3P_1$–$(8d)^3D_2$, 1122.004 Å. All three lines are produced by transitions out of excited fine-structure levels of the C I ^3P state. A detailed discussion of the large number of C I lines observed in the 1122 Å region for ζ Oph is given in de Boer and Morton (1979). The C I line at 1121.920 Å appears not to be a problem. The basis for this conclusion is that in a careful study of the Fe II profiles in a number of well-observed stars we found no convincing evidence for the existence of a strong line near 1121.92 Å, even though a C I line near this wavelength should be partially resolved from the Fe II line with the *Copernicus* resolution of 0.05 Å. However, the C I lines at 1121.998 and 1122.004 would not be resolved and could present a serious contamination problem. In the case of ζ Oph, which has an unusually strong interstellar C I absorption line spectrum, we can roughly estimate the strength of these two lines from the measured strength of other C I lines in the 1122 Å region (de Boer and Morton 1979). With the assumption of LS coupling to compute the relative line strengths we obtain W_λ (1121.998 Å + 1122.004 Å) $\approx$ 9 mÅ. Therefore contamination at the 10 mÅ level is a distinct possibility in the Fe II 1121.987 Å line equivalent widths given in Table 1. To test the effect of this C I blending we rederived Fe II column densities for the 19 stars having measurements of three Fe II lines. The rederived column densities were obtained by using only the Fe II equivalent widths for the line at 1144.946 Å to estimate the saturation correction of the weaker 1133.678 Å line. In all 19 cases the resultant logarithmic column densities were within 0.03 of the values given in Table 2 which are based on all three Fe II lines. This implies that even though C I blending may slightly increase the equivalent width of the Fe II 1121.987 Å line, the change has only a minor effect on N(Fe II). This result is most likely due to the fact that for most of the objects of Table 1, the 1133.678 Å Fe II line is only mildly saturated; hence uncertainties in W_λ (1121.987) primarily influence the derived velocity parameter, b, and only slightly modify the derived N(Fe II).

To provide information about possible contributions to N(Fe II) from H II region absorption, we obtained, for 13 objects, single U1 scans across the Fe III resonance line at 1122.526 Å. The results of these measurements are listed in Table 3 and discussed in § III*a*.

III. RESULTS

a) H I *or* H II *Region Absorption?*

Fe I, Fe II, and Fe III have ionization potentials of 7.87, 16.18, and 30.64 eV, respectively. In H I regions Fe II should be the dominant ion stage, while for H II regions Fe II, Fe III, and Fe IV will have similar column densities (Olthof and Pottasch 1975). The Fe II column

TABLE 3

Fe III MEASUREMENTS

HD	NAME	W_λ (1122.526) (mÅ)	log N(Fe III) (cm^{-2})	COMMENTS*
74375		19.0	<13.48	
112244		38.0	-	Uncertain continuum
113904B	θ Mus	107.0	-	Broad complex profile. W_λ assumes entire profile is due to Fe III.
135591		17.0	<13.43	
141637	1 Sco	<4.0	<12.81	
144217A	β^1 Sco	11.0	<13.25	
144470	ω^1 Sco	6.0	<12.98	
145502	ν Sco	<4.0	<12.81	
147933A	ζ Oph	18.0	<13.46	
148184	χ Oph	10.0	<13.21	
148605	22 Sco	<6.0	<12.98	
150898		33.0	-	Uncertain continuum
165024	θ Ara	<6.0	<12.98	

*In all cases interstellar CI absorption could contribute to the measured feature. Therefore only upper limits to N(Fe III) are computed.

densities reported in Table 2 should primarily refer to gas in the H I regions. However, contributions to N(Fe II) may occasionally occur due to absorption in H II regions (Steigman, Strittmatter, and Williams 1975). Separating H I region from H II region Fe II absorptions would be a major problem if gaseous iron exhibited little or no depletion in H II regions. However, emission-line measurements for the Orion Nebula (Olthof and Pottasch 1975) and absorption-line measurements for the H II region around ζ Oph (Morton 1975) imply that iron is depleted in H II regions by factors of 10^{-1} to 10^{-2}. If this is true of all H II regions, then the contamination of N(Fe II) by H II region absorption should not be a major problem. We note that the iron depletion in the ζ Oph H II region may be even larger than indicated, since the Fe III line measured by Morton (1975) is strongly contaminated with C I absorption (de Boer and Morton 1979).

To test for H II region contamination we obtained, for 13 of the Fe II program stars, one U1 scan across the Fe III resonance line at 1122.526 Å. This line is often blended with a C I line at 1122.518 Å. For ζ Oph de Boer and Morton (1979) estimate that about half of the reported strength of the Fe III line could be due to C I. In objects with broad interstellar lines blending by C I lines at 1122.447 and 1122.644 Å provides an additional source of uncertainty. Finally, stellar Fe III absorption sometimes provides a steeply sloped continuum and a weak stellar background. Table 3 lists for each object the Fe III equivalent width or upper limit. Even though the measurements are very uncertain due to the above-mentioned difficulties, the results are informative. In 10 cases the Fe III–C I blend was either absent or weak ($W_\lambda < 20$ mÅ). The Fe III column density upper limits listed for these objects in Table 3 assume no line saturation and $f_{1122.5} = 0.056$, a theoretical f value from Kurucz (1974). In these 10 cases the Fe III column density upper limits are smaller than the Fe II column densities of Table 2 by factors ranging from 18 to 78. If we make the assumption that Fe II and Fe III have comparable column densities in H II regions (Olthof and Pottasch 1975) we conclude for these 10 objects that H II region contributions to N(Fe II) are negligible. For the other three objects in Table 3 (HD 112244, θ Mus, and HD 150898) a relatively strong feature does exist near 1122.5 Å. For these stars we measure very uncertain Fe III equivalent widths ranging from 33 to 107 mÅ. In all cases part of the measured W_λ is probably produced by C I absorption. For these stars we definitely expect some H II region contamination of the Fe II column densities, provided in the H II regions N(Fe II) $\approx N$(Fe III). However, on intercomparing measurements in Tables 1 and 3 we note that for all three of these stars the Fe III W_λ's are ~ 2 times smaller than the W_λ's for the Fe II 1121.97 Å line, even though the latter line has an f-value ~ 3 times smaller. From these comparisons we conclude that H II region contamination is only a minor problem. As a final check, we note that if H II regions are significantly contributing to N(Fe II), we then might expect the amount of contamination to correlate with spectral type. To test this hypothesis we plotted the observed iron depletion from column (11) of Table 2 against spectral type but found no apparent correlation.

In the discussion that follows we will assume that N(Fe II) is a reliable indicator of the total H I region gaseous iron column density and that $-\log \delta = \log N(\mathrm{H\ I} + \mathrm{H_2}) - \log N(\mathrm{Fe\ II}) - 4.6$ is a reliable measure of the depletion of gaseous iron in H I regions. If the assumption that the cosmic iron abundance and the solar iron abundance are identical proves to be wrong (see § II), it will be necessary in the future to adjust the zero point of the depletion parameter. If there are variations in the total iron abundance (gas + dust), they will appear as variations in the depletion parameter.

In the expression for δ, we have assumed that H I region column densities of Fe I and Fe III are negligible compared with the column density of the dominant ion. The neglect of Fe I compared with Fe II appears justified in view of the low ionization potential of Fe I and the great difficulty in detecting optical lines for

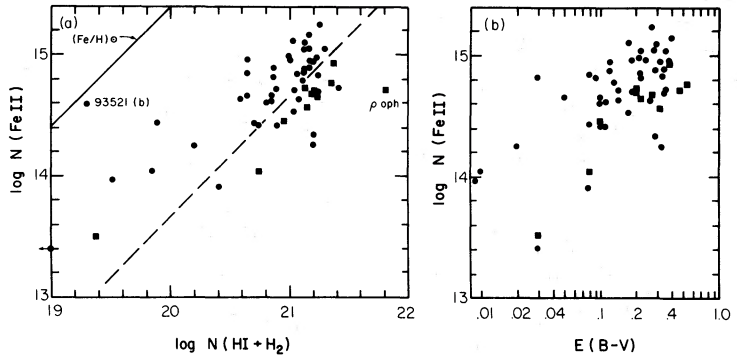

FIG. 1.—(*a*) (*left*) The logarithm of the Fe II column density is plotted against the logarithm of the total hydrogen column density. The solid line shows where the points should lie for a cosmic (assumed solar) iron abundance ratio. The dashed line is the average interstellar result, $\langle \mathrm{Fe/H} \rangle = 4.5 \times 10^{-7}$, inferred from the data. The variation about this average is large. The two extreme cases of this variation (HD 93521 and ρ Oph) are noted in the figure. (*b*) (*right*) The logarithm of the Fe II column density is plotted against $E(B - V)$. Except for the region of small $E(B - V)$ the distribution of points seen in Fig. 1*b* is roughly similar to that found in Fig. 1*a*. In both figures data points for stars in the Scorpius-Ophiuchus region are denoted by square symbols.

this ion. Fe I column densities for stars in Table 2 are: ζ Oph, N(Fe I) = 3.3×10^{11} cm^{-2}, Shulman, Bortolot, and Thaddeus (1974); ζ Per, N(Fe I) = 5.1×10^{11} cm^2, Chaffee (1974); and o Per, N(Fe I) = 9.1×10^{11} cm^{-2}, Chaffee (1974). These numbers imply Fe I/Fe II abundance ratios ranging from 4×10^{-3} to 9×10^{-4}. Therefore Fe I can be safely ignored in estimating the depletion. The neglect of N(Fe III) in H I regions is well justified in view of the 16.18 eV ionization potential of Fe II.

b) Correlations with N(H I + H$_2$) and $E(B - V)$

Figure 1*a* shows N(Fe II) correlated with the total hydrogen column density, N(H I + H$_2$) = N(H I) + $2N$(H$_2$). The solid line indicates the solar Fe/H abundance ratio of 2.5×10^{-5} (Withbroe 1971). Fe II and N(H I + H$_2$) correlate only roughly. The average abundance ratio for all the objects $\langle$Fe/H$\rangle = \sum N$(Fe II)/$\sum N$(H I + H$_2$) = 4.5×10^{-7} implies an average depletion of $\delta = 0.018$. This average (denoted by the dashed line in Fig. 1*a*) is somewhat smaller than the value $\langle$Fe/H$\rangle = 6.3 \times 10^{-7}$ obtained from low-resolution S59 spectra of 67 stars (de Boer and Lamers 1978). The variation about the average result is much larger than the estimated 1 σ error of 0.15, the total range in depletion being from $\delta = 0.78$ for component *b* of the high-latitude star HD 93521 (see § III*f*) to $\delta = 0.0032$ for ρ Oph. Ninety-five percent of the points plotted are contained in the zone defined by lines a factor of 5 higher and a factor of 3 lower than the average line. The tendency for nearby stars with small N(H I + H$_2$) to exhibit less depletion has been discussed by York (1975) and is apparent in the figure; all points with log N(H I + H$_2$) < 20.3 lie above the mean line.

The data of Table 2 provide evidence for regional differences in the amount of depletion. For example, the two Cygnus stars (68 and 69 Cyg) have $\langle\delta\rangle$ = 0.039, while the 10 Scorpius-Ophiuchus stars (excluding the nearby λ Sco) have $\langle\delta\rangle = 0.0091$. In Figure 1*a* and 1*b* the Scorpius-Ophiuchus stars are denoted with the square symbols. In all but one case these symbols lie below the average dashed line, the most extreme case being the dark cloud star ρ Oph. One might expect these regional differences in depletion to be interrelated with regional differences in extinction or polarization. This interrelation will be investigated in § III*c*.

Figure 1*b* shows N(Fe II) plotted against $E(B - V)$. This figure has the same general appearance as Figure 1*a*, which might be expected, since N(H I + H$_2$) and $E(B - V)$ are well correlated (Paper II). However, for small N(H I + H$_2$) and small $E(B - V)$ Figures 1*a* and 1*b* differ. This is possibly the result of the large relative uncertainty in $E(B - V)$ for color excesses less than about 0.1 mag.

c) Correlations of Depletion and Various Dust Parameters

In § III*b* it was demonstrated that the depletion of gaseous iron is highly variable. It is of interest to determine whether this variability is related in some way to grain characteristics along each line of sight. In this section we will therefore investigate possible relationships between δ and: (1) the shape of the interstellar extinction curve in the ultraviolet; (2) λ_{max}, the wavelength of maximum polarization which is often used as a grain size indicator; and (3) the gas-to-dust ratio as determined by the ratio N(H I + H$_2$)/$E(B - V)$.

In interpreting the various diagrams found in this and the next section, one should note that, for iron, δ varies considerably; but $(1 - \delta)$, the fraction of interstellar iron tied up in the solid phase, is nearly constant and equal to ~ 1. Therefore, if correlations are found between δ and various dust parameters, they are most likely produced for indirect reasons.

The shape of the interstellar extinction curve in the ultraviolet is complex and variable (Bless and Savage 1972). The variability is greatest in the far-ultraviolet and is presumably produced by changes in the relative numbers of the small grains required to produce a rapidly rising extinction curve with decreasing wavelength for $\lambda \lesssim 1500$ Å. The quantity $E(1330 - V)/E(B - V)$ is a measure of the far-ultraviolet extinction curve shape changes. The value for this ratio listed in column (14) of Table 2 were obtained from *OAO 2* broad-band photometry (Code, private communication). $E(1330 - V)$ refers to the extinction between a 200 Å wide band centered at 1330 Å and the usual photoelectric visual band. Depletion is plotted against $E(1330 - V)/E(B - V)$ in Figure 2*a*. A *very* rough correlation exists suggesting less depletion for larger values of $E(1330 - V)/E(B - V)$. Since the latter quantity is a measure of the *relative* numbers of small to large grains, the correlation implies that gaseous iron is removed as the small particles are removed. This suggests that the small particles are removed by grain growth and/or coalescence rather than grain destruction. Obviously the real situation is much more complex, since one can find individual data points that deviate from the above generalization.

In Figure 2*b* depletion is plotted against values of λ_{max}, the wavelength of maximum polarization. Values of λ_{max} were taken from Serkowski, Mathewson, and Ford (1975) for 16 of the objects listed in Table 2. There are only three data points in the sample with large λ_{max}, and the depletion for two of these (HD 112244 and ν Sco) appears approximately normal, while the third object (ρ Oph) has the largest depletion recorded in the sample of 55 stars. In the limited sample of data plotted in Figure 2*b* we do not see a correlation. This may imply that changes in the amount of iron depletion are not responsible for the variations in the visual polarizing properties of grains.

In Figure 2*c* depletion is compared with the gas-to-dust ratio as measured by N(H I + H$_2$)/$E(B - V)$. To reduce the scatter produced by errors in $E(B - V)$ we have only included data points with $E(B - V) \geq 0.10$. There is no apparent correlation among all the data points clustering in the upper left portion of the figure. Perhaps observational errors in both δ and N(H I + H$_2$)/$E(B - V)$ are masking a weak relation

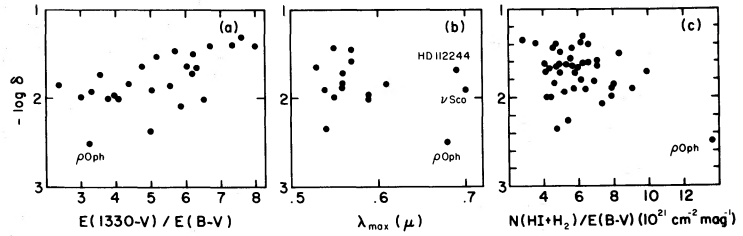

FIG. 2.—Minus the logarithm of the gaseous iron depletion is correlated with $E(1330 - V)/E(B - V)$ in Fig. 2*a*, with λ_{max} (μm) in Fig. 2*b*, and with $N(\text{H I} + \text{H}_2)/E(B - V)$ in Fig. 2*c*. $E(1330 - V)/E(B - V)$ is a measure of the amount of far-ultraviolet to visual extinction, and λ_{max} is the wavelength in microns at which the visual interstellar polarization is a maximum. Both these quantities provide indirect information about the sizes of interstellar grains along the line of sight.

between these two quantities. As usual, the data point for the dark cloud star ρ Oph falls in a discrepant part of the diagram. Although correlations are not established by individual data points, it is interesting that the object with the largest depletion has the largest value of $N(\text{H I} + \text{H}_2)/E(B - V)$. In Paper II it was noted that the large value of the gas-to-color excess ratio for this star is probably the result of a decrease in the $(B - V)$ reddening efficiency for the larger than normal sized grains in the ρ Oph cloud. In the future it will be of interest to obtain additional data on objects similar to ρ Oph. Such data may permit us to establish a connection between depletion and the gas-to-color excess ratio.

d) Correlation of Depletion and Various Cloud Parameters

If grain formation and/or destruction occurs in diffuse interstellar clouds, then one might expect to find correlations between the amount of depletion and cloud parameters (Snow 1975). In Figures 3 and 4 depletion is plotted against four different measures of the physical conditions in interstellar clouds.

In Figure 3*a*, $-\log \delta$ is plotted versus the *mean* line of sight total hydrogen density, $n(\text{H I} + \text{H}_2) = N(\text{H I} + \text{H}_2)/r$ (see column [12], Table 1; and Paper I). A rather pronounced correlation exists with higher-density regions exhibiting higher depletion. While $n(\text{H I} + \text{H}_2)$ is a rather crude indicator of the true physical density in interstellar clouds because of the inhomogeneous nature of the interstellar medium, it is significant that the observed correlation persists over a thousandfold range in $n(\text{H I} + \text{H}_2)$. In our view Figure 3*a* provides a demonstration that depletion does depend on particle density in the interstellar medium. An alternate presentation of the correlation between depletion and cloud density is illustrated in Figure 3*b*. Here we have plotted $-\log \delta$ versus $E(B - V)/r$, the reddening per unit distance to each star. Note that the result is the same; depletion correlates with $E(B - V)/r$, a measure of the mean grain number density.

In Figure 4*a*, $-\log \delta$ is plotted against $-\log f$, where $f = 2N(\text{H}_2)/[N(\text{H I}) + 2N(\text{H}_2)]$ is the fractional abundance by mass of hydrogen in the molecular form. Data points for which only upper limits to f are available are marked with arrows. The values of f were taken from Paper I and are listed in column (12) of Table 2. The equilibrium value of f is influenced by both the H_2 formation and destruction rates. However, the H_2 formation rate depends on the product of the atomic hydrogen and grain number density, hence larger values of f will tend to be associated with the densest interstellar regions. For a brief discussion of the theory of H_2 formation and destruction and a comparison of H_2 observations with theory see § III*e* in Paper I. In Figure 4*a* we note that depletion is definitely greater in those regions with large f. Figure 4*a* provides additional evidence that depletion is largest in the densest interstellar regions.

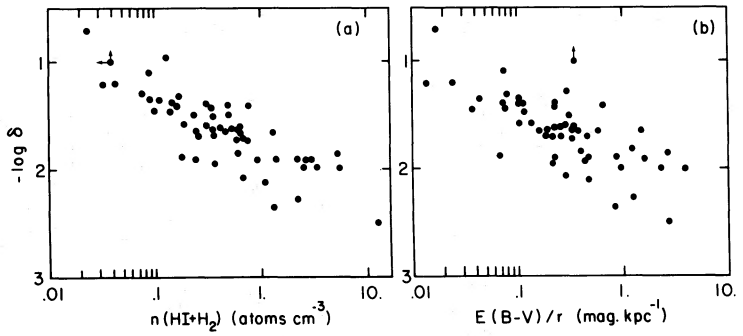

FIG. 3.—Minus the logarithm of the gaseous iron depletion is plotted against two crude indicators of line of sight density. In Fig. 3*a* (*left*) $-\log \delta$ is plotted versus the *mean* line of sight total hydrogen density in atoms cm^{-3}, while in Fig. 3*b* (*right*), $-\log \delta$ is plotted versus the reddening per unit distance in mag kpc^{-1}. In both plots, which span a large range in $n(\text{H I} + \text{H}_2)$ or $E(B - V)/r$, it is evident that depletion is greatest (smallest δ) in the densest regions.

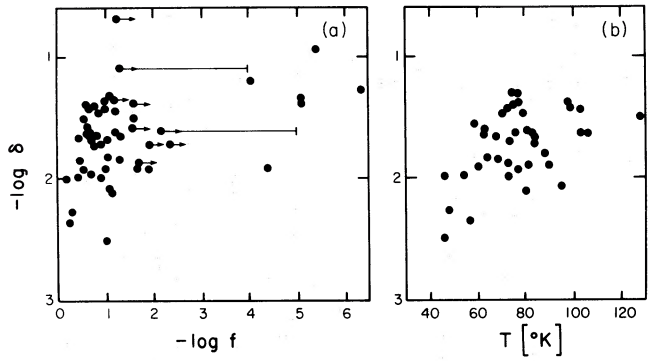

FIG. 4.—(*a*) (*left*) Minus the logarithm of the iron depletion is plotted versus $-\log f$, where $f = 2N(H_2)/[2N(H_2) + N(H\ I)]$ is the fractional abundance of hydrogen in the molecular form averaged over each line of sight. Points with arrows denote cases where curve of growth uncertainties prevent a reliable measure of $N(H_2)$ (see Paper I). In these cases the lines that extend to the right in two cases mark the corresponding lower limits to $N(H_2)$ and hence f. Since H_2 formation is favored in the densest clouds, it is important to note that the iron depletion is greatest for the objects with the largest values of f. (*b*) (*right*) Minus the logarithm of the iron depletion is plotted against cloud kinetic temperatures as inferred from the H_2 $J = 1$ to $J = 0$ population ratio (see Paper I). The coldest clouds appear to exhibit the largest depletion (smallest δ).

The correlations observed in Figures 3*a*, 3*b*, and 4*a* all imply larger amounts of depletion in the densest interstellar regions. This empirical result could be produced by a density-dependent formation process or alternately by a density-dependent destruction process. If grain growth or accretion does occur in diffuse clouds, then one would expect a greater depletion in the densest regions, since the accretion rate scales with the product of the gas and grain number density. However, one cannot use the results of Figures 3*a*, 3*b*, and 4*a* to argue that this process definitely occurs; the data could be equally well explained by a destruction process that operates more efficiently in the low-density regions. One such process would be grain destruction via particle collisions in shock waves.

In Figure 4*b*, $-\log \delta$ is plotted against the cloud kinetic temperatures as inferred from the H_2 $J = 0$ to 1 population ratio (see Paper I). The points plotted are for cases where the H_2 is strongly self-shielding [$N(H_2) \gtrsim 10^{17}$ molecules cm^{-2}]. It is only in this situation that $N(J = 1)/N(J = 0)$ is a measure of cloud kinetic temperature (Dalgarno, Black, and Weisheit 1973). Depletion does correlate roughly with T. The colder clouds exhibit larger amounts of depletion. If the interstellar medium sampled by these observations is in approximate pressure equilibrium, the colder clouds will also be the denser clouds; hence Figure 4*b* may simply represent an alternate way of plotting Figure 3*a*. However, if pressure equilibrium does not prevail, then Figure 4*b* is probably providing indirect information about the heating and cooling of interstellar clouds. As depletion increases one might naively expect the cloud temperature to increase, since important coolants are removed. However, we note that the trend exhibited in Figure 4*b* runs in the opposite sense.

e) Correlations with Other Heavy Elements

Interstellar gaseous iron exhibits a large and highly variable amount of depletion (see Fig. 1*a*). It is of interest to determine whether this variability correlates with the variable depletion found for other heavy elements. Finding correlations or a lack of correlations may provide insights about the composition of the different kinds of grains in which the various heavy elements are located. However, since correlations may simply be the result of a variety of indirect relationships between two quantities, one must be very careful in drawing conclusions from the presence or absence of a correlation. Stokes (1978) has demonstrated that column densities for Ti II and Ca II are well correlated

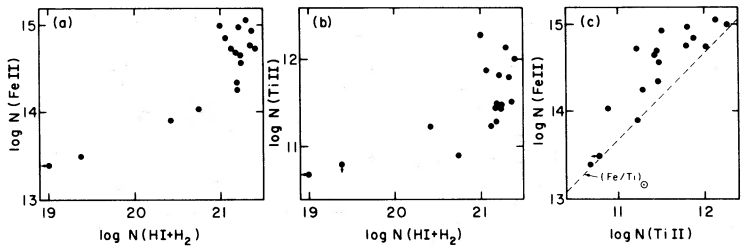

FIG. 5.—Correlations between Fe II, Ti II, and (H I + H_2) are shown for the 17 survey stars for which Ti II measurements exist (see Table 2, column [15]). (*a*) shows log N(Fe II) versus log N(H I + H_2), (*b*) shows log N(Ti II) versus log N(H I + H_2), while (*c*) shows log N(Fe II) versus log N(Ti II) and the solar ratio, $(Fe/Ti)_\odot = 460$, which is denoted by the dashed line. Fe II and Ti II correlate significantly better with each other than with hydrogen.

even though both elements exhibit large and variable amounts of depletion. In column (15) of Table 2 Ti II column densities are listed for 17 of the Fe II program stars. Most of these column densities are from Stokes (1978). The (H I + H_2), Fe II, and Ti II column densities for the same set of stars are intercompared in Figure 5*a*, *b*, and *c*. Figure 5*a* shows log N(Fe II) versus log N(H I + H_2), Figure 5*b* shows log N(Ti II) versus log N(H I + H_2), while Figure 5*c* shows log N(Fe II) versus log N(Ti II). In Figure 5*c* we have also denoted with the dashed line the solar ratio $(Fe/Ti)_\odot = 460$ (Withbroe 1971). A simple inspection of Figure 5 reveals that, while N(Fe II) and N(Ti II) correlate poorly with N(H I + H_2), these two heavy elements correlate reasonably well with each other. Since a similar result was found by Stokes (1978) for Ti II and Ca II it appears that Fe, Ti, and Ca may be located in grains with roughly similar formation and/or destruction characteristics. However, these correlations do not necessarily imply that Fe, Ti, and Ca are located in the same grain type. While the data are more uncertain, the measurements of de Boer and Lamers (1978) indicate that the comments for Fe, Ti, and Ca can be extended to include Mn.

For the data plotted in Figure 5*c* ΣN(Fe II)/ΣN(Ti II) = 950. Therefore interstellar titanium is ~2.1 times more depleted than interstellar iron.

f) *High-Latitude Stars*

Table 4 provides a list of depletion measurements for the distant high-latitude stars included in the Fe II program. The various entries are: the HD number, the galactic latitude, the stellar distance in parsec, the distance above the galactic plane in parsec, the depletion, and the average line-of-sight hydrogen density. With the exception of HD 93521 (see below), we have not attempted a separation of the observed line profiles into components. For the data generally available component separation would be difficult, since the components usually overlap and the signal-to-noise ratio is not particularly good for these relatively faint sources. All of the high-latitude objects exhibit less iron depletion than the overall average of $\delta = 0.018$ derived in § III*b*. This may be the result of a greater scale height for the gas than the dust. Alternately, the high-latitude objects generally have small n(H I + H_2) = N(H I + H_2)/r (see Table 4), and we may be simply seeing the density effect illustrated in Figure 3. The most extreme case of low depletion is the intermediate-velocity component (component *b*) toward HD 93521. For this star the Fe II data are of reasonably high quality, and in Tables 2 and 4 measurements are indicated for two components separated by 0.16 Å or 42 km s^{-1}. Optical and 21 cm radio observations toward this star have been summarized in Table 4 of Paper I. The 21 measurements permit the determination of N(H I) and hence δ in each component since f is small. In Table 4 components (*b*) and (*a*) have been identified with the Ca II components at $V_{\text{heliocentric}} = -56$ km s^{-1} and -12 km s^{-1} observed by Münch and Zirin (1961). The logarithmic H I column densities derived by Habing (1969*a*) for these two components are 19.3 for (*b*) and 19.9 for (*a*). Münch and Zirin (1961), Habing (1969*a*, *b*), and Rickard (1972) have presented evidence that the component at -56 km s^{-1} is due to gas at a distance z above the plane of more than 500 pc. For this component we have recorded the least depletion ($\delta = 0.78$) of all the objects listed in Table 2. One possible explanation for the intermediate-velocity clouds found well above the plane is that they result from galactic supernova explosions (for a review of this and other possibilities, see Verschuur 1975). It is important to note that nearly normal abundances of gaseous iron have also been found in the high-velocity clouds associated with the Vela supernova remnant (Jenkins, Silk, and Wallerstein 1976). This abundance similarity lends support to the supernova hypothesis for the production of the high-z intermediate-velocity clouds.

TABLE 4

DISTANT HIGH-LATITUDE STARS

HD	b	r (pc)	z (pc)	δ	n(H I + H_2) (cm^{-3})
93521.....	+62	1778	1570	0.14 (a) 0.78 (b)	0.023
149881.....	+36	1614	949	0.081	0.090
214080.....	−57	3404	2855	0.065	0.042
219188.....	−50	2355	1804	0.035	0.10

IV. SUMMARY OF RESULTS

By combining the new information on interstellar gaseous iron given in Tables 2 and 3 with existing optical and ultraviolet data for the same interstellar lines of sight the following results are obtained:

1) The depletion of the interstellar gaseous iron in H I regions is large and variable with an observed range from $\delta = 0.78$ to 0.0032 and an average of 0.018. These depletion results should not be significantly affected by H II region absorption.

2) There are regional differences in the iron depletion. For example, the Scorpius-Ophiuchus stars exhibit approximately 4 times more iron depletion than two Cygnus stars.

3) The amount of iron depletion correlates roughly with variations in the ultraviolet extinction properties of grains but does not appear to correlate with changes in the visual polarization properties of grains or with variations in the total gas-to-color excess ratio.

4) Several crude indicators of interstellar cloud density imply that iron depletion is greater in the denser interstellar regions. This result could be explained by either density-dependent formation processes or density-dependent destruction processes.

5) Iron depletion is greatest in the interstellar clouds with the lowest kinetic temperatures.

6) While Fe and Ti both exhibit large and variable depletions, column densities for these two elements are reasonably well correlated. Since a similar result

was found for Ti and Ca (Stokes 1978) and for Fe and Mn (de Boer and Lamers 1978), it appears that Fe, Ca, Mn, and Ti may be contained in grains with similar formation and/or destruction properties.

7) Iron depletion is found to be less in the clouds toward distant high-latitude stars. The most notable example is the intermediate-velocity cloud toward HD 93521 for which a nearly normal gaseous iron abundance is obtained. The normal iron abundance found in this cloud and in galactic supernova remnants lends support to a supernova origin of the intermediate-velocity clouds found well above the galactic plane.

This observing program was made possible by the enthusiastic support of the Princeton *Copernicus* staff and especially Drs. T. Snow and D. York. Dr. J. Drake was instrumental in developing the efficient observing routines and in seeing that the program stars were included in the busy *Copernicus* schedule. We acknowledge helpful comments concerning the first draft of the manuscript from Drs. K. de Boer, E. Churchwell, and J. Mathis. Mr. K. Feggans provided very helpful support in processing and organizing the spectra. B. D. S. acknowledges support for this study through NASA grants NSG 5100 and NSG 5181.

REFERENCES

Bless, R. C., and Savage, B. D. 1972, *Ap. J.*, **171**, 293.
Bohlin, R. C., Savage, B. D., and Drake, J. F. 1978, *Ap. J.*, **224**, 132 (Paper II).
Chaffee, F. H. 1974, *Ap. J.*, **189**, 427.
Cohen, J. G. 1974, *Ap. J.*, **194**, 37.
Dalgarno, A., Black, J. H., and Weisheit, J. C. 1973, *Ap. Letters*, **14**, 77.
de Boer, K. S. 1979, *Ap. J.*, in press.
de Boer, K. S., and Lamers, H.J.G.L.M. 1978, *Astr. Ap.*, **69**, 327.
de Boer, K. S., and Morton, D. C. 1979, *Astr. Ap.*, in press.
de Boer, K. S., Morton. D. C., Pottasch, S. R., and York, D. G. 1974, *Astr. Ap.*, **31**, 405.
de Boer, K. S., and Pottasch, S. R. 1974, *Astr. Ap.*, **36**, 463.
Field, G. B. 1974, *Ap. J.*, **187**, 453.
Habing, H. J. 1969*a*, *Bull. Astr. Inst. Netherlands*, **20**, 128.
———. 1969*b*, *Bull. Astr. Inst. Netherlands*, **20**, 177.
Hobbs, L. M. 1974, *Ap. J.*, **191**, 381.
Jenkins, E. B., Drake, J. F., Morton, D. C., Rogerson, J. B., Spitzer, L., and York, D. G. 1973, *Ap. J.* (*Letters*), **181**, L122.
Jenkins, E. B., Silk, J., and Wallerstein, G. 1976, *Ap. J. Suppl.*, **32**, 681.
Kurucz, R. L. 1974, *Smithsonian Ap. Obs. Spec. Rept.* No. 360.
Marschall, L. A., and Hobbs, L. M. 1972, *Ap. J.*, **173**, 43.
Morton, D. C. 1975, *Ap. J.*, **197**, 85.
Morton, D. C., and Hu, E. M. 1975, *Ap. J.*, **202**, 638.
Münch, G., and Zirin, H. 1961, *Ap. J.*, **133**, 11.
Nachman, P., and Hobbs, L. M. 1973, *Ap. J.*, **173**, 43.
Olthof, H., and Pottasch, S. R. 1975, *Astr. Ap.*, **43**, 291.
Pagel, B. E. J. 1974, paper presented at NATO Advan. Study Inst. on the Origin and Abundance of Chemical Elements, Cambridge, England.
Rickard, J. J. 1972, *Astr. Ap.*, **17**, 425.
Rogerson, J. B., Spitzer, L., Drake, J. F., Dressler, K., Jenkins, E. B., Morton, D. C., and York, D. G. 1973, *Ap. J.* (*Letters*), **181**, L97.
Savage, B. D., Bohlin, R. C., Drake, J. F., and Budich, W. 1977, *Ap. J.*, **216**, 291 (Paper I).
Savage, B. D., and Jenkins, E. B. 1972, *Ap. J.*, **172**, 491.
Serkowski, K., Mathewson, D. S., Ford, V. L. 1975, *Ap. J.*, **196**, 261.
Shull, J. M. 1977, *Ap. J.*, **212**, 102.
Shull, J. M., and York, D. G. 1977, *Ap. J.*, **211**, 803.
Shull, J. M., York, D. G., and Hobbs, L. M. 1977, *Ap. J.* (*Letters*), **211**, L139.
Shulman, S., Bortolot, B. J., and Thaddeus, P. 1974, *Ap. J.*, **193**, 97.
Snow, T. P. 1975, *Ap. J.* (*Letters*), **202**, L87.
———. 1976, *Ap. J.*, **204**, 759.
———. 1977, *Ap. J.*, **216**, 724.
Spitzer, L., and Jenkins, E. B. 1975, *Ann. Rev. Astr. Ap.*, **13**, 133.
Steigman, G., Strittmatter, P. A., and Williams, R. E. 1975, *Ap. J.*, **198**, 575.
Stokes, G. M. 1978, *Ap. J. Suppl.*, **36**, 115.
Stokes, G. M., and Hobbs, L. M. 1976, *Ap. J* (*Letters*), **208**, L95.
Verschuur, G. 1975, *Ann. Rev. Astr. Ap.*, **13**, 257.
Wallerstein, G., and Goldsmith, D. 1974, *Ap. J.*, **187**, 237.
Withbroe, G. D. 1971, *The Menzel Symposium: NBS Spec. Publ. no. 353*, ed. K. B. Gebbie (Washington: Government Printing Office).
York, D. G. 1975, *Ap. J.* (*Letters*), **196**, L103.
Zeippen, C. J., Seaton, M. J., and Morton, D. C. 1977, *M.N.R.A.S.*, **181**, 527.

R. C. BOHLIN: NASA Goddard Space Flight Center, Code 681, Greenbelt, MD 20771

B. D. SAVAGE: Department of Astronomy, Sterling Hall, University of Wisconsin, Madison, WI 53706